Phase Separation during the Topotactic Reduction of the Pyrochlore $Y_2Ti_2O_7$

Michael A. Hayward†

Inorganic Chemistry Laboratory, Department of Chemistry, University of Oxford, South Parks Road, Oxford, OX1 3QR U.K.

Received October 11, 2004. Revised Manuscript Received November 17, 2004

The topotactic reduction of the pyrochlore $Y_2Ti_2O_7$ with CaH_2 is described. Neutron and X-ray powder diffraction data reveal the reduction yields mixtures of two reduced phases: $Y_2Ti_2O_{6.48(2)}$, a material from which oxide ions have been removed from the 48f anion site, and $Y_2Ti_2O_{5.90(6)}$, which exhibits a small amount of cation antisite disorder and a complicated defect anion structure. An electronic origin for the observed phase separation is explored. Magnetic data collected from reduced samples are consistent with delocalized metallic behavior.

Introduction

The low-temperature topotactic reduction of complex metal oxides offers a powerful route to prepare new solid phases with unusual cation coordinations and oxidation states.[1,2] In these syntheses oxide ions are removed from substrate oxides by the action of reducing agents to yield structurally related phases with significant anion vacancy concentrations. It therefore follows that one of the restrictions of this reaction type is that the substrate oxide phase contains a reducible metal cation with a high coordination number. The tendency of the $A_2B_2O_6O'$ pyrochlore structure to stabilize the high oxidation states of cations on the 6-coordinate B-site makes phases of this type obvious substrates for topotactic reduction reactions.

In addition to oxidation state arguments, there are strong structural motivations for exploring the reduction chemistry of pyrochlores. The pyrochlore structure can be considered to be an ordered anion-deficient variant of the fluorite structure. The ordered removal of 1/8 of the anions from the fluorite structure leads to the formation of two crystallographically distinct cation sites: the 8-coordinate ($6 \times O + 2 \times O'$) 16d A-site and the 6-coordinate ($6 \times O$) 16c B-site. The resulting tetrahedral connectivity of both the A and B cation sublattices leads to strong geometric frustration in antiferromagnetically ordered systems.[3] Extensive studies focusing on phases with magnetic centers on the A-site have revealed a wide range of physical behavior including phases with macroscopically degenerate ground states as described by "spin-ice" models.[4] There are however relatively few examples of materials which have magnetic ions only on the B-site (rather than on both the A- and B-sites). The two best known examples, $Y_2Mo_2O_7$ and $Y_2Ru_2O_7$, exhibit magnetic behavior consistent with transitions to spin-glass states at 22 and 80 K, respectively,[5,6] which is surprising in the absence of any crystallographic disorder in these materials.[7,8] This study of the reduction chemistry of $Y_2Ti_2O_7$ was motivated by the observation that the topotactic removal of the O′ oxide ion from this Ti^{IV} phase would result in the formation of $Y_2Ti_2O_6$, which would contain a tetrahedrally connected array of $S = 1/2$ Ti^{III} B-site cations.

Table 1. Synthesis Conditions and Measured Stoichiometries of Samples Prepared

sample	conditions	average stoichiometry
A	3×2 days, 575 °C	$Y_2Ti_2O_{6.36}$
B	4×3 days, 575 °C	$Y_2Ti_2O_{6.20}$
C	3×7 days, 575 °C	$Y_2Ti_2O_{5.99}$

Experimental Section

By the use of a standard ceramic route, 5 g samples of $Y_2Ti_2O_7$ were prepared from Y_2O_3 (99.999%, Alfa Aesar) and TiO_2 (99.99%, Aldrich). Stoichiometric ratios of the dried binary oxides were thoroughly mixed in an agate pestle and mortar, pressed into 13 mm pellets, and heated in air at 1350 °C for 3×3 days to yield a white single phase product, confirmed by powder X-ray diffraction. The reduction of $Y_2Ti_2O_7$ was performed with CaH_2 (>95%, Aldrich); 2:1 stoichiometric ratios of CaH_2:$Y_2Ti_2O_7$ were thoroughly ground in an argon glovebox and sealed under vacuum in a fused silica tube of approximate 60 cm^3 volume. Samples were then heated as described in Table 1. After reaction, samples were washed in a nitrogen atmosphere with a 4-fold molar excess of 0.1 M NH_4Cl in methanol, to remove the calcium-containing phases, and then pure methanol before being dried under vacuum. Complete removal of calcium-containing phases was confirmed by EDX

† Telephone: +44 1865 272623. Fax: +44 1865 272690. E-mail: michael.hayward@chem.ox.ac.uk.

(1) Hayward, M. A. *Chem. Commun.* **2004**, 170.
(2) Hayward, M. A.; Green, M. A.; Rosseinsky, M. J.; Sloan, J. *J. Am. Chem. Soc.* **1999**, *121*, 8843.
(3) Greedan, J. E. *J. Mater. Chem.* **2001**, *11*, 37.
(4) Bramwell, S. T.; Gingras, M. J. P. *Science* **2001**, *294*, 1495.
(5) Dunsiger, S. R.; Kiefl, R. F.; Chow, K. H.; Gaulin, B. D.; Gingras, M. J. P.; Greedan, J. E.; Keren, A.; Kojima, K.; Luke, G. M.; MacFarlane, W. A.; Raju, N. P.; Sonier, J. E.; Uemura, Y. J.; Wu, W. D. *Phys. Rev. B* **1996**, *54*, 9019.
(6) Taira, N.; Wakeshima, M.; Hinatsu, Y. *J. Solid State Chem.* **1999**, *144*, 216.
(7) Reimers, J. N.; Greedan, J. E.; Sato, M. *J. Solid State Chem.* **1988**, *72*, 390.
(8) Lee, J. S.; Noh, T. W.; Bae, J. S.; Yang, I.; Takeda, T.; Kanno, R. *Phys. Rev. B* **2004**, *69*, 214428.

10.1021/cm048220p CCC: $30.25
Published on Web 01/13/2005

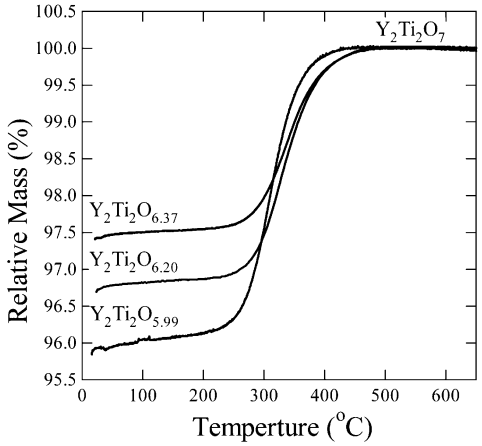

Figure 1. Relative mass gain as a function of temperature for samples heated under oxygen.

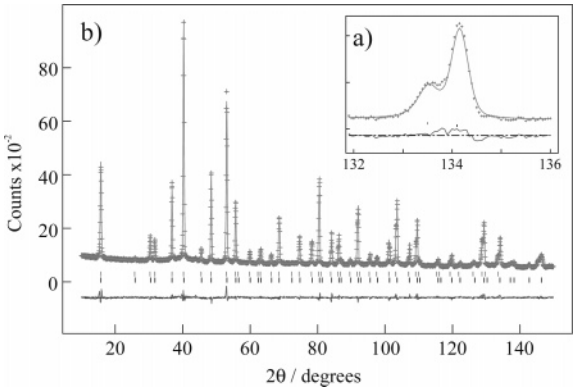

Figure 2. Observed, calculated, and difference plots for a two-phase refinement against neutron powder diffraction data collected from $Y_2Ti_2O_{6.20}$. (a) An expanded high-angle region emphasizing the two-phase nature of the sample.

measurements. Powder diffraction data suitable for structural refinement were collected using a PANalytical X'Pert Pro X-ray diffractometer (monochromatic Cu $K\alpha_1$) and station D2b ($\lambda = 1.59$ Å) at the ILL neutron source, Grenoble. All structural refinements were performed using the GSAS suite of programs.[9] Thermogravimetric data were collected from powder samples using a Rheometric Scientific STA 1500 thermal analyzer. Direct current (dc) magnetic susceptibility data were collected between 5 and 300 K using a Quantum Design MPMS SQUID magnetometer. Room temperature two-probe conductivity measurements were performed on powder samples compressed between two copper pistons within an insulating sleeve.

Results

Structural and Chemical Characterization. The reaction between $Y_2Ti_2O_7$ and CaH_2 at 575 °C converts the white mixture of powders into a black material. X-ray powder diffraction data collected, prior to washing with acid, allow the identification of three phases in the reaction product: CaH_2, CaO, and a cubic phase which can be readily indexed in the $Fd\bar{3}m$ space group. This suggests that the reaction shown in eq A has occurred to yield a topotactically reduced pyrochlore phase $Y_2Ti_2O_{7-x}$.

$$Y_2Ti_2O_7 + CaH_2 \rightleftharpoons Y_2Ti_2O_{7-x} + xCaO + xH_2 \quad (A)$$

Thermogravimetric data collected while heating samples under flowing oxygen (Figure 1) show these reduced materials can be readily converted back to stoichiometric $Y_2Ti_2O_7$ (confirmed by X-ray powder diffraction) and give the stoichiometries indicated for each of the three samples in Table 1.

Close inspection of both X-ray and neutron powder diffraction data reveal that the diffraction reflections observed for each of the three samples are split. The splitting observed could not be readily accounted for by any simple crystallographic distortion; however, a good fit to the data could be achieved with a model consisting of two different reduced pyrochlore phases (Figure 2a). Models consisting of two reduced pyrochlore phases were therefore refined against diffraction data from each of the three samples prepared. To increase the stability of the refinements, the thermal parameters of corresponding sites in the two phases were constrained to be identical as were the instrumental contributions to the peak shape functions of both phases. At convergence the two-phase models provided a relatively good fit to the diffraction data; however, there were a number of statistically significant deviations particularly in fits to the neutron diffraction data. The recent report on the analogous reduced lutetium and ytterbium titanium pyrochlores $Lu_2Ti_2O_{6.10}$ and $Yb_2Ti_2O_{6.45}$[10] observed a small amount of metal antisite disorder accompanied by the partial occupation of 48f and 32e defect anion sites. These features were added to the structural models with significant improvements to the fitting statistics of all three samples. Refinement of the fractional occupancy of the 8b O(1) anion site resulted in values which were slightly greater than unity (~1%); therefore this site was set to full occupation in the final refinement cycles. Results of the structural refinements are given in Table 2 with selected bond lengths in Table 3. A plot comparing the agreement between the data and model for $Y_2Ti_2O_{6.20}$ is shown in Figure 2b.

The results of the structural refinements (Table 2) clearly show that all three samples are mixtures of the same two reduced phases of approximate composition $Y_2Ti_2O_{6.48(2)}$ and $Y_2Ti_2O_{5.90(6)}$. The different mean oxygen stoichiometries observed for the three samples are due to differing molar ratios of these two phases between samples.

Phase 1 has a simple structure based on that of the fully oxidized starting material $Y_2Ti_2O_7$. On reduction oxide ions are removed exclusively from the 48f sites to yield a phase of composition $Y_2Ti_2O_{6.48(2)}$. The removal of these oxide ions and the associated reduction of the titanium centers from a mean oxidation state of +4 to +3.5 leads to an expansion in the lattice parameter and average Ti−O bond length consistent with the larger ionic radius of Ti^{III} compared with Ti^{IV}. The average titanium coordination number is 5.49(3), which can be interpreted as a 1:1 ratio of 5- and 6-coordinate sites (Figure 3a,b). Bond valence sums for these two coordinations are calculated to be +3.13 and +3.76, respectively, giving a mean titanium oxidation state (+3.44) close

(9) Larson, A. C.; Von Dreele, R. B. Los Alamos National Laboratory: Los Alamos, 1994.

(10) Blundred, G. D.; Bridges, C. A.; Rosseinsky, M. J. *Angew. Chem.* **2004**, *116*, 3646.

Table 2. Results of Rietveld Refinements Performed against Neutron and X-ray Powder Diffraction Data for the Three Samples Prepared

Sample A

atom	site	x	y	z	U_{equiv} (Å^2)	occupancy
Ti	16c	0	0	0	0.0178	1
Y	16d	0.5	0.5	0.5	0.0165	1
O(1)	8b	0.375	0.375	0.375	0.0124	1
O(2)	48f	0.33109(6)	0.125	0.125	0.0139	0.915(5)
		a = 10.09666(7); composition: $Y_2Ti_2O_{6.49(2)}$; mole fraction: 66.6%				
Ti/Y	16c	0	0	0	0.0178	0.927(3)/0.073(3)
Y/Ti	16d	0.5	0.5	0.5	0.0165	0.927(3)/0.073(3)
O(1)	8b	0.375	0.375	0.375	0.0124	1
O(2)	48f	0.3395(2)	0.125	0.125	0.0139	0.741(4)
O(3)	32e	−0.409(2)	0.159(2)	−0.409(2)	0.0139	0.042(4)
O(4)	48f	0.408(3)	0.125	0.125	0.0139	0.050(4)

a = 10.1197(1); composition: $Y_2Ti_2O_{5.91(6)}$; mole fraction: 33.3%
overall sample composition: $Y_2Ti_2O_{6.29(4)}$
TGA: $Y_2Ti_2O_{6.37(2)}$
χ^2 = 3.4, Rp = 4.2%, wRp = 3.9%

Sample B

atom	site	x	y	z	U_{equiv} (Å^2)	occupancy
Ti	16c	0	0	0	0.0210	1
Y	16d	0.5	0.5	0.5	0.0192	1
O(1)	8b	0.375	0.375	0.375	0.0138	1
O(2)	48f	0.33165(7)	0.125	0.125	0.0179	0.914(3)
		a = 10.09557(5); composition: $Y_2Ti_2O_{6.48(2)}$; mole fraction: 48.7%				
Ti/Y	16c	0	0	0	0.0210	0.949(2)/0.051(2)
Y/Ti	16d	0.5	0.5	0.5	0.0192	0.949(2)/0.051(2)
O(1)	8b	0.375	0.375	0.375	0.0138	1
O(2)	48f	0.3399(1)	0.125	0.125	0.0179	0.762(4)
O(3)	32e	−0.409(3)	0.159(3)	−0.409(3)	0.0179	0.030(2)
O(4)	48f	0.412(2)	0.125	0.125	0.0179	0.036(2)

a = 10.11924(7); composition: $Y_2Ti_2O_{5.90(5)}$; mole fraction: 51.3%
overall sample composition: $Y_2Ti_2O_{6.18(4)}$
TGA: $Y_2Ti_2O_{6.20(2)}$
χ^2 = 1.94, Rp = 4.1%, wRp = 4.2%

Sample C

atom	site	x	y	z	U_{equiv} (Å^2)	occupancy
Ti	16c	0	0	0	0.0205	1
Y	16d	0.5	0.5	0.5	0.0191	1
O(1)	8b	0.375	0.375	0.375	0.0199	1
O(2)	48f	0.3311(2)	0.125	0.125	0.0237	0.914(3)
		a = 10.0975(1); composition: $Y_2Ti_2O_{6.48(2)}$; mole fraction: 19.2%				
Ti/Y	16c	0	0	0	0.0205	0.929(2)/0.071(2)
Y/Ti	16d	0.5	0.5	0.5	0.0191	0.929(2)/0.071(2)
O(1)	8b	0.375	0.375	0.375	0.0199	1
O(2)	48f	0.3395(1)	0.125	0.125	0.0237	0.739(4)
O(3)	32e	−0.4055(9)	0.1555(9)	−0.4055(9)	0.0237	0.049(2)
O(4)	48f	0.404(2)	0.125	0.125	0.0237	0.048(2)

a = 10.12658(8); composition: $Y_2Ti_2O_{5.91(6)}$; mole fraction: 80.8%
overall sample composition: $Y_2Ti_2O_{6.01(6)}$
TGA: $Y_2Ti_2O_{5.99(2)}$
χ^2 = 1.39, Rp = 4.0%, wRp = 3.9%

to that expected from the crystallographic stoichiometry (+3.48(2)). The mean coordination number of yttrium is 7.49(3), consisting of 2 O(1) and 5.49 O(2) ligands. This suggests a 1:1 ratio of 7- and 8-coordinate Y^{III} with bond valence sums of +2.71 and +3.00, respectively (Figure 3c,d).

Phase 2 has a more complicated structure due to the presence of metal antisite disorder and the associated occupation of defect anion positions labeled O(3) and O(4) according to the scheme presented by Blundred et. al.[10] In this more reduced phase between 5 and 7% of the metal cations are on the "wrong" crystallographic site and the occupation of the two defect oxygen sites can be rationalized on the basis of the coordination requirements of the two different metal cations. The 48f O(2) and 48f O(4) sites lie spatially very close to each other (0.69 Å in sample A) and have complementary bond lengths to the 16c and 16d metal sites such that O(2) forms coordination spheres suitable for Ti at 16c and Y at 16d and O(4) suitable for Y at 16c and Ti at 16d (Table 3). We can therefore consider the O(2) and O(4) sites as lying at the extremes of a region of scattering which accounts for a 48f site that is displaced locally depending on the identity of the metal ions on the surrounding 16-fold sites.

The defect 32e site is derived from the 8a site, about which it is tetrahedrally disposed. The 8a site is vacant in the pyrochlore structure and coordinates only to the 16c cation

Table 3. Selected Bond Lengths Obtained from Rietveld Refinements Performed against Neutron and X-ray Powder Diffraction Data for the Three Samples Prepared

	bond length (Å)		
	sample A	sample B	sample C
	Phase 1		
Ti−O(2)	1.964(1)	1.966(1)	1.964(1)
Y−O(1)	2.186(1)	2.186(1)	2.186(1)
Y−O(2)	2.469(1)	2.464(1)	2.469(1)
	Phase 2		
Ti(16c)−O(2)	2.005(1)	2.007(1)	2.007(1)
Ti(16c)−O(3)	2.06(1)	2.07(3)	2.076(9)
Ti(16c)−O(4)	2.40(1)	2.42(1)	2.37(1)
Y(16d)−O(1)	2.191(1)	2.191(1)	2.192(1)
Y(16d)−O(2)	2.416(1)	2.413(1)	2.418(1)
Y(16d)−O(4)	2.012(9)	1.998(9)	2.03(1)

site in an analogy to the 8b and 16d sites. Indeed, full occupation of the 8a site would make the two 16-fold positions crystallographically equivalent, suggesting that occupation of this position by oxide ions is in response to the coordination requirements of antisite Y^{III} ions on the 16c site. The slight displacement which lowers the symmetry from 8a to 32e means that anions located in these positions bridge only two 16c centers rather than four.

We can therefore construct coordination spheres around the two 16-fold sites. If we consider the data from sample A, the 16d site contains 92% Y and 8% Ti and has a mean coordination number of 6.74. This corresponds to a 3:1 ratio of 7- and 6-fold sites. All the 16d sites are coordinated by two 8b O(1) ions and the majority by five additional 48f ions (from the O(2) and O(4) sites). One-fourth of the sites have only four 48f ligands, and it would be expected that the titanium ions would reside predominantly in these 6-coordinate positions (Figure 4a,b).

The 16c site is slightly more complicated. The average coordination number of this site is 4.99, consisting of 4.74 48f ligands and 0.25 32e O(3) ligands. We can therefore construct a model in which 3/4 of the 16c sites are surrounded by five 48f oxide ions with 1/4 surrounded by four 48f and one 32e oxide ions to yield two distinct 5-fold coordinations. However, due to the metal antisite disorder, this would imply that the 8% Y^{III} present on the 16c site would be 5-coordinate with bond valence sums of +1.766 (5 × 48f ligands) or +2.27 (4 × 48f, 1 × 32e ligands). Given the relationship between the 32e site and the higher symmetry 8b site mentioned previously, it is reasonable to associate the occupation of the 32e site with the presence of Y^{III} in the 16c position. Thus, we might expect Y^{III} to have a (4 × 48f, 2 × 32e) coordination with a more physically reasonable

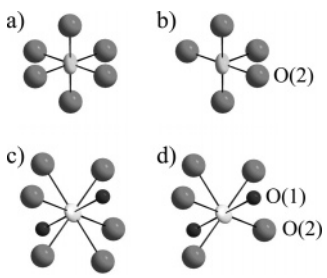

Figure 3. Local coordination environments for cations in $Y_2Ti_2O_{6.5}$. (a, b) The 6- and 5-coordinate geometries of titanium. (c, d) The 8- and 7-coordinate geometries of yttrium.

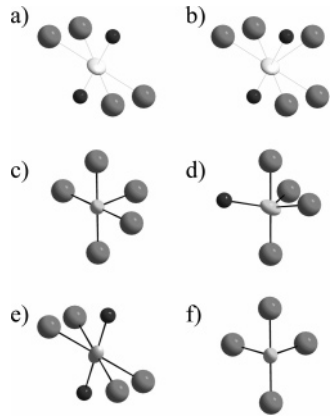

Figure 4. Local coordination environments for cations in $Y_2Ti_2O_{5.9}$. (a, b) The 6- and 7-coordinate geometries of the 16d site. (c, d) The two 5-fold geometries of the 16c site. (e) The 6-coordinate 16c site occupied by yttrium. (f) The 4-coordinate 16c site.

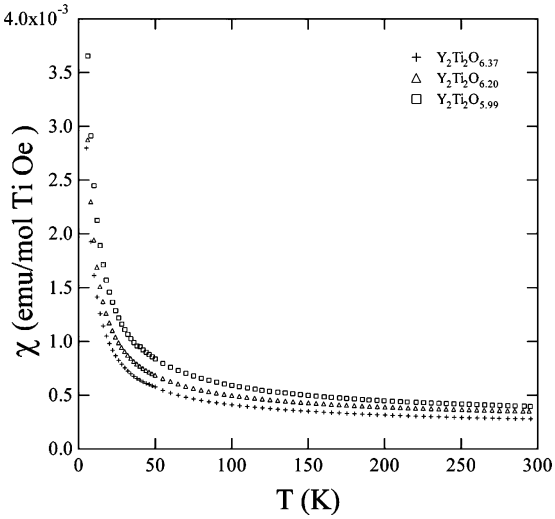

Figure 5. Plot of zero-field-cooled magnetic susceptibility of $Y_2Ti_2O_{7-x}$ as a function of temperature.

bond valence sum of +3.13. The formation of such a 6-fold site means that for each Y^{III} antisite defect two (4 × 48f, 1 × 32e) and one 4-coordinate (4 × 48f) titanium sites are produced as shown in Figure 4c−f.

Physical Characterization. Zero-field-cooled and field-cooled dc magnetic susceptibility data were collected from all three samples in an applied field of 1000 Oe, as a function of temperature. The field-cooled and zero-field-cooled data were identical for all three samples, so only the zero-field-cooled are shown in Figure 5 for clarity. All three data sets were readily fitted by a Curie−Weiss model with a temperature-independent term ($\chi = \chi_0 + C/(T - \theta)$) over the temperature range $5 < T/\mathrm{K} < 300$; the results are given in Table 4. The fitting data clearly show that both the Curie term and temperature-independent susceptibility of $Y_2Ti_2O_{7-x}$ increase with x, which is consistent with the introduction of electrons into titanium d-states on reduction. However, the Curie terms of all three samples are much smaller than would be expected for a system in which the titanium d-electrons act as simple localized spins. The data are more consistent with a low level (4−6%) of Ti^{III} $S = 1/2$ weakly interacting ($\theta \approx -1.4$ K) localized impurity centers, with the spins from the remainder of the electrons introduced on reduction not being observed. An equally weak magnetic moment has been

Table 4. Results of Fits to Magnetic Data and Resistivity Measurements Collected from $Y_2Ti_2O_{7-x}$ Samples

	sample A	sample B	sample C
C	0.0158(1)	0.0189	0.0244(2)
θ	−1.27(7)	−1.44(7)	−1.43(8)
χ_0	0.000242(2)	0.000298(2)	0.000334(3)
fraction of localized $S = 1/2$	0.0421	0.0504	0.0650
maximum resistivity (295K) (Ωm)	56(2)	14(2)	13(2)

observed for $Y_2Nb_2O_7$ which has been explained by the adoption of a strongly correlated spinless insulating ground state in this phase.[11] The reduced phases reported here, however, have a positive temperature-independent magnetic moment (as opposed to the negative value observed for $Y_2Nb_2O_7$) with magnitudes similar to those reported for metallic $La_xSr_{1-x}TiO_3$ ($0.75 < x < 1$)[12] (Table 4). Room temperature resistivity measurements from cold-pressed powder samples also indicate a modest conductivity for the reduced samples of $\sim 6 \times 10^{-2}\ \Omega^{-1}\ m^{-1}$ compared with $<10^{-5}\ \Omega^{-1}\ m^{-1}$ for $Y_2Ti_2O_{7.00}$ (Table 4). It should be stressed these are minimum bounds on the conductivity as there are likely to be large contributions from poor intergrain contacts. The magnetic and transport data suggest one possible explanation for the small observed magnetic moment is that the majority of the electrons introduced on reduction are delocalized in a metallic manner. Neutron powder diffraction data collected at 300 and 5 K show no evidence for long-range antiferromagnetic order, negating an alternate possibility that low moments are observed due to strong antiferromagnetic coupling in the temperature range studied.

The weak magnetic behavior of $Y_2Ti_2O_{7-x}$ is in strong contrast to that reported for $Lu_2Ti_2O_{7-x}$, which exhibits a magnetic susceptibility consistent with strongly antiferromagnetically coupled local moments for both $x = 0.9$ and 0.5 ($\theta = 176$ and 227 K for $x = 0.9$ and 0.5, respectively).[10]

Discussion

The structural refinements show that all three samples prepared are mixtures of the same two $Y_2Ti_2O_{7-x}$ phases. This phase separation suggests there is a phase gap in the composition range $Y_2Ti_2O_{7-x}$ ($0.5 < x < 1.1$). That is, there are values of x for which there are no stable phases with the pyrochlore structure under the reaction conditions employed. Attempts to prepare single-phase samples by annealing these mixtures were unsuccessful. Heating samples under vacuum at temperatures below 700 °C resulted in no change observable by X-ray powder diffraction. Annealing above 700 °C led to complete phase separation to $Y_2Ti_2O_{7.00}$ and the cubic perovskite $YTiO_3$.

Close inspection of the two pyrochlore phases that bound the unstable composition region does not reveal any obvious crystallographic explanation for the instability of compositions in this range, so electronic band structure calculations were performed in order to explore an electronic origin for the instability. To this end the band structure of $Y_2Ti_2O_{7.00}$ was calculated using the STUTTGART TB-LMTO-ASA program employing 72 irreducible k points.[13] Figure 6 shows a plot of the total and partial density of states (DOS) for the unreduced material $Y_2Ti_2O_{7.00}$. The calculated DOS show the Fermi energy (E_F) lies at the top of the largely oxygen 2p valence band with a large band gap to the predominantly titanium 3d conduction band. These observations are consistent with $Y_2Ti_2O_7$ being a white insulating material and provide confirmation that on reduction electrons will be inserted into states which are predominantly titanium 3d in character.

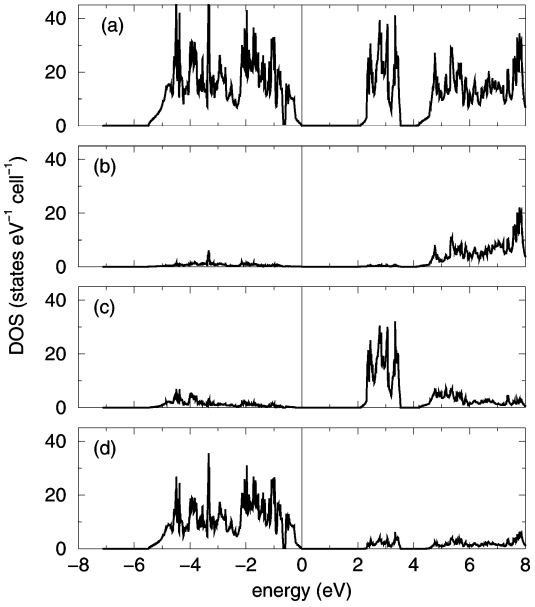

Figure 6. Calculated DOS as a function of energy. (a) All states; (b) yttrium 4s; (c) titanium 3d; (d) oxygen 2p.

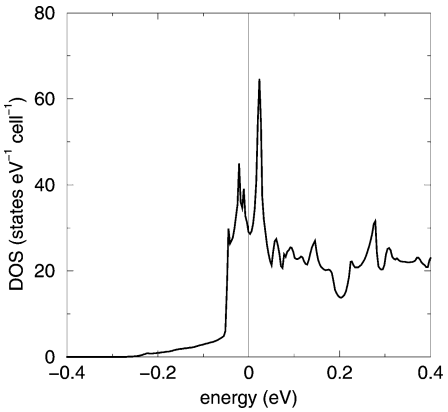

Figure 7. Calculated total DOS for $Y_2Ti_2O_6F$ as a function of energy.

To avoid the complications associated with the disordered vacancies present in the oxygen lattice of $Y_2Ti_2O_{6.5}$, calculations were performed using the isoelectronic phase $Y_2Ti_2O_6F$, in which the 8b oxide ion is replaced with a fluoride ion, to model this phase. Figure 7 shows the total calculated DOS for $Y_2Ti_2O_6F$, and by analogy that of $Y_2Ti_2O_{6.5}$. It can clearly be seen that the Fermi energy has now moved up into the titanium 3d valence band, on the introduction of one electron per formula unit, and that E_F lies in a local minimum just

(11) Fukazawa, H.; Maeno, Y. *Phys. Rev. B* **2003**, *67*, 54410.
(12) Tokura, Y.; Taguchi, Y.; Okada, Y.; Fujishima, Y.; Arima, T.; Kumagai, K.; Iye, Y. *Phys. Rev. Lett.* **1993**, *70*, 2126.
(13) Jepsen, O.; Andersen, O. K. MPI fuer Festkoerperforschung: Stuttgart, 2000.

below a large narrow peak in the calculated total DOS. Simple integration reveals that this peak corresponds to 0.48 state (0.96 electron) per formula unit; therefore, the expected position of E_F for $Y_2Ti_2O_{5.9}$ lies at a higher energy than this feature. It therefore seems likely that the observed phase gap is related to an instability associated with the high DOS at E_F that phases in the range $Y_2Ti_2O_{7-x}$ ($0.5 < x < 1.1$) would have.

Conclusion

The low-temperature topotactic reduction of $Y_2Ti_2O_7$ with calcium hydride yields a mixture of two reduced pyrochlore phases ($Y_2Ti_2O_{6.5}$ and $Y_2Ti_2O_{5.9}$) which bound a region of unstable composition ($Y_2Ti_2O_{7-x}$, $0.5 < x < 1.1$). Magnetic susceptibility data are consistent with metallic delocalized behavior in these phases. Such behavior suggests that phases of the form $Y_2Ti_2O_{7-x}$ are unlikely to be good model systems for the study of geometrically frustrated magnetism.

Acknowledgment. I thank R. Seshadri for assistance with the electronic structure calculations, T. Hansen for assistance collecting the neutron powder diffraction data, and the Royal Society for funding this work.

CM048220P